Evaluation of [C(sp3)/[C(sp2)] ratio in diamondlike films through the use of a complex dielectric constant

Evaluation of the [C(sp^3)]/[C(sp^2)] ratio in diamondlike films through the use of a complex dielectric constant

F. Demichelis, C. F. Pirri, and A. Tagliaferro
Dipartimento di Fisica del Politecnico di Torino, corso Duca degli Abruzzi 24, 10 129 Torino, Italy
(Received 9 September 1991)

The evaluation of the amount of tetrahedral and trigonal cross-linking, that is, the sp^3- and sp^2-hybridized carbon, is of great importance in understanding the properties of amorphous carbon films. In this paper we report a method for deducing the $[sp^3]/[sp^2]$ ratio from the experimental values of the complex dielectric constant as obtained by optical transmittance and reflectance measurements. We assume a Gaussian-like distribution of π and π^* electronic densities of states in order to fit the contribution of $\pi \rightarrow \pi^*$ to the imaginary part, ϵ_2, of the dielectric constant in the low-energy region. Through the Kramers-Kronig relationships we deduce the corresponding values of the real part ϵ_1 of the dielectric constant for such transitions. By subtracting these values from the measured ϵ_1 we deduce the contribution of $\sigma \rightarrow \sigma^*$ to ϵ_1. The Wemple-Didomenico model has been used to obtain the dispersion energy and the average excitation energy. Knowing the plasmon energies, we apply the "f-sum rule" to deduce the $[sp^3]/[sp^2]$ ratio. The method applied to a-C:H films deposited by rf diode sputtering provides results in agreement with those obtained by other techniques.

I. INTRODUCTION

It is known that carbon atoms can form bonds with three different types of hybridization: tetrahedral sp^3, leading to a three-dimensional diamondlike (DL) network; trigonal sp^2, leading to a two-dimensional graphitelike layered structure; and linear sp^1, which results in one-dimensional acetylenelike structure.

Hydrogenated amorphous carbon (a-C:H) is a material whose characteristics represent a mixing of the properties of the structurally ordered solids diamond, graphite, and hydrocarbon polymers. Thus its structure cannot easily be classified. While in glassy carbon 100% sp^2 sites and, in a-C, only up to 10% sp^3 sites are present, a-C:H contains a mixture of sp^3 and sp^2 sites in comparable amounts. The presence of two bonding types prevents the formation of parallel graphitic layers.[1] Moreover, sp^2 and sp^3 sites in a-C:H are somewhat segregated and clustered.[2]

The a-C:H films with DL properties, due to an unusually large number of sp^3 bonds, have attracted much interest in the past few years. Their optical and electrical properties appear to be determined by the relative amounts of sp^3 and sp^2 sites. For this reason, evaluation of the $[sp^3]/[sp^2]$ ratio in these films is important. Many different techniques have been proposed and applied in order to obtain quantitative data on carbon bonding. Quantitative information on the relative concentrations of sp^3-, sp^2-, and sp^1-hybridized carbon has been obtained through use of infrared (ir) spectroscopy[3] and electron-energy-loss spectroscopy (EELS),[4,5] as well as through use of nuclear magnetic resonance[6,7] (NMR) and Raman spectroscopy.[8] However, some of these techniques have inherent limitations.

Infrared spectroscopy provides information through the deconvolution of the C-H stretching peak (2900–3100 cm^{-1}) into individual contributions correlated to the different bonding environment of C-H bonds.[3] This method does not allow one to elicit information on the sites where C is not bonded to H. Moreover, it is quite difficult to observe C-C vibrations (especially for sp^3 sites).

Electron-energy-loss spectroscopy requires *in situ* measurements of scattered electrons on very thin films (< 50 Å), if information on the whole thickness is required. *In situ* measurements are needed to ensure the cleanliness of the surface. Owing to the different sputtering yields of graphitic and DL zones, measurements performed on samples cleaned by sputtering cannot be relied on.

Nuclear-magnetic-resonance measurements represent the more precise and bulk-sensitive method; NMR can be used to obtain information on hydrogen bonded to different sites as well. However, large amounts (> 50 mg) of material are required. This is a major drawback for films whose deposition rate is generally well below 0.1 μm/min. Moreover, the amount of material needed increases as the hydrogen content decreases.[7]

Raman spectroscopy can only be used to obtain a qualitative indication of the amount of graphitization in the film.[8]

A method based on determining the energy dependence of the imaginary part of the dielectric constant, ϵ_2, has also been used.[9] The effective number of π electrons is evaluated by comparing the ϵ_2 first moment for a-C:H to that of graphite. However, no information on sp^3 sites or on σ bonds is obtained, and knowledge of ϵ_2 values up to at least 8 eV is needed, since the energy dependence of ϵ_2 for graphite and a-C:H at energies below 7 eV is quite different.[9]

The aim of the present work is to analyze the dielectric constants in order to obtain directly a reliable value of the $[sp^3]/[sp^2]$ ratio. The ϵ_2 curves, as functions of photon energy, show two peaks, one at low energies (< 5 eV), arising from $\pi \rightarrow \pi^*$ interband transitions, and the other

at higher energies (> 10 eV), arising from $\sigma \rightarrow \sigma^*$ interband transitions.[2]

The contribution of the low-energy peak ($\pi \rightarrow \pi^*$ transitions) to ϵ_1 is taken into account through the Kramers-Kronig[10] relationships. The contribution of $\sigma \rightarrow \sigma^*$ transitions to ϵ_1 is analyzed with the Wemple-Didomenico model.[11] From the parameters of this model, the number of σ electrons is obtained. By using this value and the f-sum rule for $\pi \rightarrow \pi^*$ transitions,[10] the $[sp^3]/[sp^2]$ ratio is evaluated.

In order to estimate better the plasmon energy of π electrons, use of the Gaussian band approximation is made for π bands.[12] A discussion of the different models of the dielectric constant for amorphous semiconductors and of their applicability to a-C:H is also presented.

II. EXPERIMENT

Films were deposited by means of sputter-assisted plasma chemical-vapor-deposition system. A graphite target was sputtered in an argon-hydrogen atmosphere.[13] Hydrogen content in the atmosphere was varied in order to obtain different $[sp^3]/[sp^2]$ ratios in the films.[12]

Optical measurements were performed using a uv-visible near-infrared Perkin-Elmer Lambda 9 spectrophotometer in the wavelength range 190–2500 nm on films deposited on Suprasil quartz. The optical data were analyzed using standard routines.[13] Values of the refractive index (n) and of the extinction coefficient (k) were extracted. From their values, real and imaginary parts of the dielectric constants were readily determined, since

$$\epsilon_1(E)=n^2(E)-k^2(E) ,$$
$$\epsilon_2(E)=2n(E)k(E) . \tag{1}$$

The thicknesses of the films were determined both from the interference fringes in the transmittance spectra (for thick films)[13] and by using a Dektak II Stylus profilometer (for thin and thick films).

Data from Ref. 9 are used as well. This is done in order to verify the model and to compare the results obtained on samples deposited by different techniques.

III. DENSITY OF STATES AND OPTICAL TRANSITIONS IN a-C:H

The density of states (DOS) near the Fermi level of a-C:H is quite different from that of amorphous semiconductors,[12] such as a-Si:H and its alloys, since a-C:H is supposed to be composed of graphitic islands embedded in a DL matrix.[2]

The bands of a-C:H can be considered a weighted average of the bands of the two phases. For energies near Fermi energy, however, no contribution form the diamond phase is expected.

In the graphitic islands, the "valence band" is formed by a σ band (well below the Fermi level) and a π band (near the Fermi level). In a similar manner, the "conduction band" is formed by a π^* band (near the Fermi level) and a σ^* band (well above the Fermi level). Their energy overlap is limited to the region around 4 eV below (valence) and above (conduction) the Fermi level. The bands of the DL matrix are similar to those of diamond, since C-H bonds give rise to states having energies higher than C-C ones.

In a recent paper,[13] Gaussian shapes, symmetrical with respect to the Fermi level (E_π being the energy of the maximum and σ_π the width of the peak), were proposed as first approximations for the π and π^* bands. In that case, only the shape of the bands less than 2 eV apart from the Fermi level was considered. Here we extend the validity of the approximation, in the sense that we assume the Gaussian curves to be representative of the entire π and π^* bands (see below). In such a case, the contribution of $\pi \rightarrow \pi^*$ transitions to ϵ_2 is given by

$$\epsilon_2(E)=\frac{A}{E^2}\operatorname{erf}\left[\frac{E}{2\sigma_\pi}\right]\exp\left[-\left[\frac{2E_\pi-E}{2\sigma_\pi}\right]^2\right] . \tag{2}$$

Optical transitions are essentially local events, so the largest part of the transitions takes place from a filled state in a phase (graphitic or diamond) to an empty state in the same phase. As a consequence, the contribution of "interphase" transitions can be neglected and the two phases can be considered separately.

For low photon energies (< 5 eV), absorption takes place mainly in the graphitic islands ($\pi \rightarrow \pi^*$ transitions). In the intermediate-energy region (5–8 eV) we expect contributions from both the islands ($\sigma \rightarrow \pi^*$ and $\sigma \rightarrow \pi^*$ transitions) and from the diamond phase. Since the binding energy of σ bonds of sp^2 sites is higher than that of diamond sites, the contribution from $\sigma \rightarrow \sigma^*$ transitions in the graphitic islands becomes important at higher photon energies (> 8 eV).

IV. THE DIELECTRIC CONSTANT AND ITS MOMENTA

ϵ_1 and ϵ_2, the real and imaginary parts of the dielectric constant, are related through the Kramers-Kronig relationships:[10]

$$\epsilon_1(E)=1+\frac{2}{\pi}\int_0^\infty E'\frac{\epsilon_2(E')}{(E')^2-E^2}dE' , \tag{3a}$$

$$\epsilon_2(E)=\frac{2}{\pi}E\int_0^\infty \frac{\epsilon_1(E')}{(E')^2-E^2}dE' . \tag{3b}$$

Among the optical parameters of a thin film, however, the imaginary part of the dielectric constant is the one more directly correlated to the DOS.[14] In fact, as far as disordered materials are concerned, since the electron momentum is not a relevant quantum number, we can write (at 0 K)

$$\epsilon_2(E)=\text{const}\times\int_{E_F}^{E_F+E} Q^2(Z,E)N_o(Z-E)N_u(Z)dZ , \tag{4}$$

where E is the photon energy, $N_o(Z-E)$ is the density of

occupied states, $N_u(Z)$ is the density of unoccupied states, and E_F is the Fermi-level energy. $Q(Z,E)$ is the dipole matrix element of the optical transition, given by

$$Q(Z,E)=\langle u^*(Z)|q\mathbf{r}|o(Z-E)\rangle \ , \tag{5}$$

where q is the proton charge and $\mathbf{r}$ is the position operator.

We now wish to justify (at least qualitatively) the neglect of the contribution coming from $\pi\rightarrow\sigma^*$ and $\sigma\rightarrow\pi^*$ transitions inside graphitic islands.

The dipole matrix elements for $\pi\rightarrow\pi^*$ and $\sigma\rightarrow\sigma^*$ transitions are non-null, since these are allowed transitions and the occupied and unoccupied orbitals have a strong overlap. As far as the transitions (not forbidden by selection rules) from π to σ^* states and from σ to π^* states are concerned, we can observe that the reduced spatial overlapping of π molecular orbitals (MO's) and σ MO's strongly reduces the magnitude of the matrix element.

We can then assume that the contributions of $\sigma\rightarrow\sigma^*$ and $\pi\rightarrow\pi^*$ transitions to ϵ_2 can be separated; that is,

$$\epsilon_2(E)=\epsilon_{2\pi}(E)+\epsilon_{2\sigma}(E) \ , \tag{6a}$$

$$\epsilon_2(E)=A_\pi\int_0^\infty Q_\pi^2(Z,E)N_{o\pi}(Z-E)N_{u\pi}(Z)dE + A_\sigma\int_0^\infty Q_\sigma^2(Z,E)N_{o\sigma}(Z-E)N_{u\sigma}(Z)dE \ . \tag{6b}$$

The term $\epsilon_{2\sigma}$ is the sum of the contributions due to transitions both inside islands and inside DL matrices. However, since ϵ_2 is measured only up to a few eV, the two contributions cannot be distinguished. For this reason, we will consider $\sigma\rightarrow\sigma^*$ transitions as a whole.

The ith-order moment of ϵ_2 is defined as

$$M_i=\frac{2}{\pi}\int_0^\infty E^i\epsilon_2(E)dE \ . \tag{7}$$

It follows that the f-sum rule for the plasmon energy[10] can be written as

$$(\hbar\omega_p)^2=M_1 \ . \tag{8}$$

It is worth noting that the plasmon energy is proportional to the number of valence electrons, n_v:

$$(\hbar\omega_p)^2=Kn_v \ . \tag{9}$$

From Eq. (3a) we obtain the moment of order -1 as given by

$$M_{-1}=\epsilon_1(0)-1 \ , \tag{10}$$

where $\epsilon_1(0)$ is the static dielectric constant.

The upper limit of the momenta defining integrals can be varied. For instance, if we set its value to 8 eV, we expect that mainly $\pi\rightarrow\pi^*$ transitions contribute to the value of M_1. This assumption is the basis of the method for evaluating the number of π electrons in Ref. 9. However, as stated above, we expect a non-negligible contribution from the $\sigma\rightarrow\sigma^*$ transitions in sp^3 regions at energies higher than 7 eV (the region more heavily weighted in M_1). This fact reduces the reliability of the results obtained.

Of course, the upper limit of the integral defining M_{-1} can also be varied. In this case, however, the more heavily weighted region of ϵ_2 is the low-energy one, so that a reliable value of the contribution of $\pi\rightarrow\pi^*$ transitions to $\epsilon_1(0)-1$ can be obtained even if the upper limit of the integral is set to 5–6 eV.

V. MODELS OF THE DIELECTRIC CONSTANT

Since the dielectric constant is strictly correlated to the material properties, several attempts have been made to extract information about the material DOS from the dielectric constant. Several models have been proposed. We will briefly discuss those most used in the field of amorphous semiconductors, in the light of their application to a-C:H and of their relevance to our method.

A. Penn model

The Penn model[15] was developed for crystalline semiconductors. Its main feature is the assumption that the DOS is formed by two δ-function-like bands whose energy spacing is E_P (the so-called Penn gap). In this case, from Eqs. (4), (3a), and the sum rule (10), one obtains

$$\epsilon_1(0)=1+B\left[\frac{\hbar\omega_p}{E_P}\right]^2 , \tag{11}$$

where $\hbar\omega_p$ is the plasmon energy, $\epsilon_1(0)$ the static dielectric constant, and B is a factor of the order of unity.[16] The value of E_P can be evaluated as

$$E_P=\frac{\hbar\omega_p}{\sqrt{\epsilon_1(0)-1}} \ . \tag{12}$$

If we consider only the contribution of $\pi\rightarrow\pi^*$ transitions to ϵ_2—that is, if we deal only with $\epsilon_{2\pi}$—we can use Eq. (11) to work out the value of Penn gap for π states. The results obtained for several films are reported in Fig. 1, where the E_P values are plotted as functions of the energy spacing $2E_\pi$ between π- and π^*-band maxima. The data are well fitted by the linear relationship

$$E_P=0.143+0.924\times 2E_\pi \ . \tag{13}$$

We can conclude that the Penn gap is a useful and meaningful parameter that characterizes the energy spac-

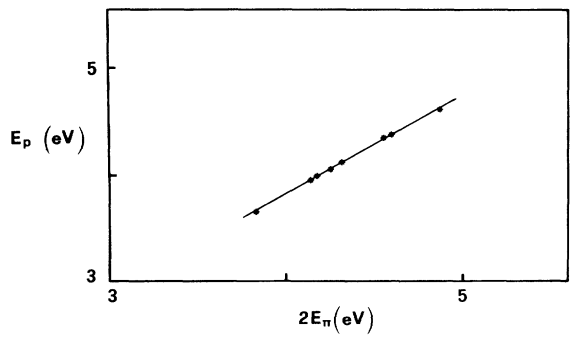

FIG. 1. Penn gap (E_P) as a function of the energy spacing $2E_\pi$ between π and π^* Gaussian band maxima.

ing between the π- and π^*-band maxima having Gaussian shapes.

B. Wemple-Didomenico model

In the Wemple-Didomenico model[11] information on the intensity and energy of interband transitions is gained through the analysis of the real part of the dielectric constant in the low-energy region. Although presented in the original paper in a different way, the basic assumptions are equivalent to the following.

(a) ϵ_2 is δ shaped:

$$\epsilon_2(E)=\frac{\pi}{2}E_d\delta(E-E_0)\ , \tag{14}$$

where E_d is the dispersion energy (proportional to the intensity of the transitions) and E_0 is the spacing between bands.

(b) The δ-shaped ϵ_2 is placed at an energy well above the energy region in which ϵ_1 is analyzed.

The δ-shaped spectrum substitutes for the true ϵ_2 spectrum, so that from this model only general information about the intensity and the interband energy spacing of the transitions can be obtained. (For a more accurate discussion, see Ref. 11.)

Evaluating ϵ_1 from Eq. (3a), the following expression is obtained:

$$\frac{1}{\epsilon_1(E)-1}=\frac{E_0}{E_d}-\frac{E^2}{E_0E_d}\ . \tag{15}$$

When conditions (a) and (b) above are fulfilled, a plot of $(\epsilon_1-1)^{-1}$ versus E^2 yields the values of E_0 and E_d, giving valuable information on the intensity (E_d) of interband transitions and on the average spacing between bands (E_0).

Before discussing the applicability of this model to *a*-C:H, we wish to recall two relationships that will be useful in the following:

$$(\hbar\omega_p)^2=M_1=E_0E_d\ , \tag{16a}$$

$$\epsilon_1(0)-1=M_{-1}=\frac{E_d}{E_0}\ . \tag{16b}$$

As far as DL *a*-C:H is concerned, a relevant absorption coefficient ($>10^2$ cm^{-1}) is usually present down to energies lower than 1 eV (corresponding to a wavelength higher than 1.24 μm). This means that, even when data in the energy region below 1 eV are considered, condition (b) is not fulfilled. The Wemple-Didomenico plot of typical DL *a*-C:H, reported in Fig. 2, clearly shows the inadequacy of this model to describe DL *a*-C:H, at least when a large amount of sp^2-hybridized bonds are present. This is a consequence of the presence in the DOS, near the Fermi level, of the π and π^* bands.

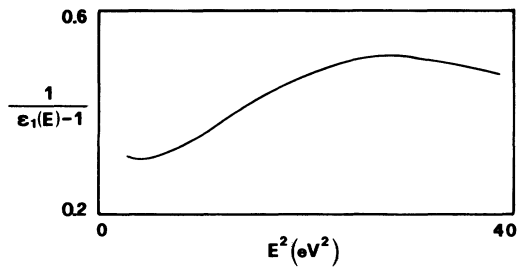

FIG. 2. Wempel-Didomenico plot of a typical DL *a*-C:H film.

VI. METHOD FOR THE DETERMINATION OF THE [sp^3]/*i*[sp^2] RATIO

We have seen above that the contribution to ϵ_2 due to electronic transitions from states in one phase (graphitic or DL) to states in another phase is negligible.

Inserting Eq. (6b) into Eq. (3a), we can separate the contributions of $\pi\rightarrow\pi^*$ and $\sigma\rightarrow\sigma^*$ transitions to $\epsilon_1(E)$:

$$\epsilon_1(E)=1+\frac{2}{\pi}\int_0^\infty E'\frac{\epsilon_{2\pi}(E')}{(E')^2-E^2}dE' + \frac{2}{\pi}\int_0^\infty E'\frac{\epsilon_{2\pi}(E')}{(E')^2-E^2}dE'\ . \tag{17}$$

By using the expressions

$$\epsilon_{1\pi}(E)-1=\frac{2}{\pi}\int_0^\infty E'\frac{\epsilon_{2\pi}(E')}{(E')^2-E^2}dE'\ , \tag{18a}$$

$$\epsilon_{1\sigma}(E)-1=\frac{2}{\pi}\int_0^\infty E'\frac{\epsilon_{2\sigma}(E')}{(E')^2-E^2}dE'\ , \tag{18b}$$

we can see that

$$\epsilon_1(E)-1=[\epsilon_{1\pi}(E)-1]+[\epsilon_{1\sigma}(E)-1]\ . \tag{19}$$

$\epsilon_2(E)$ is known, so our task now is to separate the contributions due to the different transitions. For this purpose, we will proceed as follows.

(a) We fit the low-energy region ($E<4$ eV) of the $\epsilon_2(E)$ spectra with the formula obtained from the convolution of the Gaussian bands [Eq. (2)], thereby obtaining the parameters E_π and σ_π of the Gaussian-like bands and the scale factor A.

(b) Equation (2) is assumed to describe $\epsilon_{2\pi}(E)$ for all energies.

(c) The quantity $\epsilon_{1\pi}(E)-1$ is evaluated using Eq. (18a). Since $\epsilon_1(E)-1$ has been experimentally determined, $\epsilon_{1\sigma}(E)-1$ can be evaluated in the same energy range in which optical measurements have been performed [Eq. (19)].

Most of the $\sigma\rightarrow\sigma^*$ transitions lie in an energy range well above the energy range of our optical data, so no direct information can be obtained. However, we can analyze the $\epsilon_{1\sigma}(E)-1$ energy dependence by using the Wemple-Didomenico model.

From the plot of $1/[\epsilon_{1\sigma}(E)-1]$, the parameters E_0 and E_d (Ref. 11) can be determined as stated above,

$$(\hbar\omega_p)_\sigma^2=\frac{E_d^2}{\epsilon_{1\sigma}(0)-1}\ . \tag{20}$$

Using Eq. (9), we obtain

$$n_{v\sigma}=K^{-1}\frac{E_d^2}{\epsilon_{1\sigma}(0)-1}\ , \tag{21}$$

where (E_0E_d) is the slope of the interpolating line in the Wemple-Didomenico plot.

The number of valence π electrons can be determined as follows. The plasmon energy of the π electrons is

$$(\hbar\omega_p)_\pi^2=Kn_{v\pi}=M_{1\pi}\ , \tag{22}$$

where $M_{1\pi}$ is the first moment of $\epsilon_{2\pi}(E)$. This evaluation is approximate in that the Gaussian approximation for π bands, which was proved to be satisfactory for the regions of the bands near the Fermi level,[12] has not been tested for the regions outside the Fermi-level valley.

Finally, dividing Eq. (22) by Eq. (21),

$$\frac{n_{v\pi}}{n_{v\sigma}}=\frac{M_{1\pi}}{E_dE_0}\ . \tag{23}$$

Each sp^2 site gives rise to three σ states and one π state, while each sp^3 site gives rise to four σ states and each H atom to a single σ state. Then, we can write

$$n_{v\pi}=Nf_2\ , \tag{24a}$$

$$n_{v\sigma}=N(4f_3+3f_2+f_{\rm H})\ , \tag{24b}$$

where N is the atomic density, and f_3, f_2, and $f_{\rm H}$ the C sp^3, C sp^2, and H atomic fractions, respectively. We obtain

$$\frac{n_{v\pi}}{n_{v\sigma}}=\frac{f_2}{4f_3+3f_2+f_{\rm H}}=\alpha\ . \tag{25a}$$

With the condition

$$f_3+f_2+f_{\rm H}=1\ , \tag{25b}$$

we obtain

$$f_2=(4-3f_{\rm H})\frac{\alpha}{1+\alpha}\ , \tag{26a}$$

$$f_3=\frac{(1-3\alpha)-f_{\rm H}(1-2\alpha)}{1+\alpha}\ . \tag{26b}$$

Finally, the ratio $[sp^3]/[sp^2]$ is obtained:

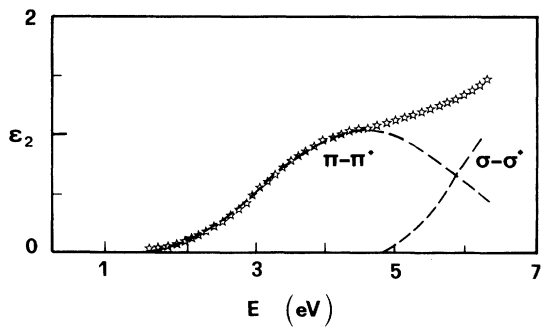

FIG. 3. Experimental ϵ_2 spectrum ($\star$) for a typical a-C:H film deconvoluted in $\epsilon_{2\pi}$ and $\epsilon_{2\sigma}$ contributions.

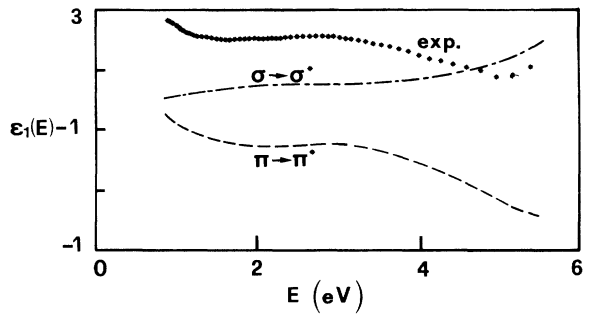

FIG. 4. Experimental $\epsilon_1(E)-1$ ($*$) and its decompostion in $\sigma\rightarrow\sigma^*$ and $\pi\rightarrow\pi^*$ contributions for a typical a-C:H film.

$$f_{3/2}=\frac{f_3}{f_2}=\frac{(1-3\alpha)-f_{\rm H}(1-2\alpha)}{\alpha(4-3f_{\rm H})}\ . \tag{27}$$

VII. RESULTS

In this section we present the results of the application of the above-outlined method to a-C:H films. In Fig. 3 an ϵ_2 spectrum for a typical a-C:H film is reported. The contributions of $\epsilon_{2\pi}$ and $\epsilon_{2\sigma}$ to the total ϵ_2 are evaluated by fitting the data in the low-energy region by Eq. (2) and by Eq. (6a), respectively. Although no long-range order in the diamond phase and some distortions of the bond parameters are expected, the onset of the $\epsilon_{2\sigma}$ contribution should not be very far from the diamond-gap value. In fact, it can be observed that the contribution of $\epsilon_{2\sigma}$ becomes relevant for energies of the order of the diamond gap.

The experimental $\epsilon_1(E)-1$ and the calculated $\epsilon_{1\pi}(E)-1$ and $\epsilon_{1\sigma}(E)-1$ curves are presented in Fig. 4. If we look at these curves from the perspective of the Wemple-Didomenico model, we see that the behaviors of $\epsilon_1(E)$ and $\epsilon_{1\pi}(E)$ are not acceptable. On the other hand, $\epsilon_{1\sigma}(E)$ is "well shaped," as can be more readily seen in Fig. 5, where a Wempel-Didomenico plot of $\epsilon_{1\sigma}(E)$ is reported. In fact, the interpolating line well approximates the data on a wide energy range, up to the highest measured energy. It should be noted that the energy range of linearity of the plot can be different for different films. This is a consequence of the different behavior of ϵ_2 at energies higher than 5 eV (see caption of Fig. 3).

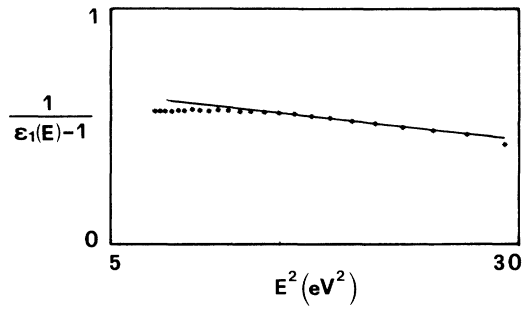

FIG. 5. Wemple-Didomenico plot for $\epsilon_{1\sigma}(E)$.

TABLE I. Wemple-Didomenico- and Penn-model parameters, $[sp^3]/[sp^2]$ ratio, and hydrogen content for several a-C:H samples. (See Sec. II for an explanation of sample nomenclature.)

Samples	E_0 (eV)	E_d (eV)	$\hbar\omega_p$ (eV)	E_P (eV)	$[sp^3]/[sp^2]$	H content (at. %)
CH1	9.38	13.85	3.22	4.31	2.06	25
CH2	8.16	14.09	3.38	3.63	1.50	25
S2	7.34	13.22	4.09	3.97	0.94	4
S5	8.57	16.34	3.58	4.02	1.88	12
S6	8.50	13.65	3.26	4.33	1.83	18
S7	8.30	15.07	3.33	4.08	1.96	13
S8	7.49	12.69	3.01	3.93	1.70	20
S9	9.06	13.14	3.10	4.56	2.10	25

From the plot of Fig. 5 the parameters E_0 and E_d are determined. Their values are reported in Table I, together with the values of the $[sp^3]/[sp^2]$ ratio. Our films are labeled by CH. For the films of Ref. 9 we have used S followed by the number identifying the film in the source paper. The trend of the $[sp^3]/[sp^2]$-ratio values is the same as that obtained with the method described in Ref. 9. This indicates that the present method is reliable at least as far as a relative value of the $[sp^3]/[sp^2]$ ratio for different films is required.

To check if the values obtained are meaningful from an absolute point of view, we have performed NMR and ir spectroscopy measurements on films deposited under the same conditions, but thicker than those used in the present work. We have seen that our method gives results comparable to those obtained by ir spectroscopy and higher than those obtained using NMR. As far as optical methods are concerned, we observe that the values obtained using the method of Ref. 9 are much higher than those obtained using the present method (see Table I). This means that the agreement of values obtained using the method of Ref. 9 with NMR data is poorer than those obtained using the present method.

We have estimated the accidental error arising from the measurements and the arbitrariness of the fitting to a Gaussian shape to be around 10%. We think that the main source of systematic error is the assumption that the matrix elements for $\pi\rightarrow\pi^*$ and $\sigma\rightarrow\sigma^*$ transitions are equal.

We wish to clarify that our method is not a purely optical one, since knowledge of the atomic percentage of hydrogen is required. However, most of the DL carbon films obtained so far have hydrogen contents ranging from 20 to 30 at. %, so that, as a first attempt, the value of 0.25 can be assumed for f_H.

VIII. CONCLUSIONS

We have shown that knowledge of the dielectric constants of a-C:H films in the photon-energy range 1–6 eV allows one to evaluate (when the hydrogen content is known) the amount of sp^3- and sp^2-hybridized atoms and the value of the $[sp^3]/[sp^2]$ ratio.

Our procedure can be outlined as follows: starting from the experimental values of the real and imaginary parts of the dielectric constant, assuming a Gaussian-like distribution for π and π^* bands and making use of both the Kramers-Kronig relationships and the Wemple-Didomenico model, the $[sp^3]/[sp^2]$ ratio is deduced.

Our method provides results in agreement with those obtained from ir measurements and generally higher than those obtained from NMR measurements. It is simple and convenient for application to both thin and thick films and furnishes data averaged over the thickness of the film.

We have shown that the contribution of $\pi\rightarrow\sigma^*$ and $\sigma\rightarrow\pi^*$ transitions can be neglected. Then, the degree of arbitrariness in the fit of ϵ_2 starting from Gaussian bands and the assumption that the matrix elements for $\pi\rightarrow\pi^*$ and $\sigma\rightarrow\sigma^*$ transitions are equal will be main sources of error. Several attempts have shown that the first factor can cause, at most, an error of 10%. The assumption regarding matrix elements is a source of systematic error and can be dealt with only if reasonable estimates of their values can be obtained in an independent way.

[1]D. A. Anderson, Philos. Mag. **35**, 17 (1977).
[2]J. Robertson, Adv. Phys. **35**, 317 (1986).
[3]B. Dischler, A. Bubenzer, and P. Koidl, Solid State Commun. **48**, 105 (1983).
[4]J. Fink, Th. Muller-Heinzerling, J. Pfluger, B. Scheerer, B. Dischler, P. Koidl, A. Bubenzer, and R. E. Sah, Phys. Rev. B **30**, 4713 (1984).
[5]J. Fink. Th. Muller-Heinzerling, J. Pfluger, A. Bubenzer, P. Koidl, and G. Grecelnis, Solid State Commun. **47**, 687 (1988).
[6]S. Kaplan, F. Jansen, and J. Machonkin, Appl. Phys. Lett. **47**, 750 (1985).
[7]A. Grill, B. S. Meyerson, V. V. Patel, J. A. Reimer, and M. A. Petrich, J. Appl. Phys. **61**, 2874 (1987).
[8]A. Reyes-Mena, J. Gonzales-Hernandez, and R. Asomoza, in *Amorphous Hydrogenated Carbon Films,* edited by P. Koidl and P. Oelhafen, Proceedings of European Materials Research Society Symposia (Les Editions de Physique, Paris, 1987), Vol. XVII, p. 229.
[9]N. Savvides, in *Amorphous Hydrogenated Carbon Films* (Ref. 8), Vol. XVII, p. 275.
[10]*Handbook of Optical Constants of Solids,* edited by E. D. Pawlik (Academic, New York, 1985), p. 38.

[11]S. H. Wemple and M. Didomenico, Phys. Rev. B **3**, 1338 (1971).
[12]D. Dasgupta, F. Demichelis, C. F. Pirri, and A. Tagliaferro, Phys. Rev. B **43**, 2131 (1991).
[13]F. Demichelis, G. Kaniadakis, A. Tagliaferro, and E. Tresso, Appl. Opt. **26**, 1737 (1987).
[14]G. D. Cody, in *Hydrogenated Amorphous Silicon*, Vol. 21B of *Semiconductor and Semimetals*, edited by J. J. Pankove (Academic, New York, 1984), p. 11.
[15]D. R. Penn, Phys. Rev. **128**, 2093 (1962).
[16]N. M. Ravindra, C. Ance, J. P. Ferraton, A. Donnadieu, and S. Robin, Phys. Status Solidi B **115**, 347 (1983).